Letters

An Integrated EMI Choke for Differential-Mode and Common-Mode Noise Suppression

Rixin Lai, Yoann Maillet, Fred Wang, Shuo Wang, Rolando Burgos, and Dushan Boroyevich

***Abstract*—This letter presents a novel integration approach for the electromagnetic interference choke. A low-permeability differential-mode (DM) choke is placed within the open window of the common-mode (CM) choke. Both chokes share the same winding structure. With the proposed approach, the footprint of inductors is greatly reduced, and high-DM inductance can be achieved. First, small-signal measurement is carried out to demonstrate the design concept and the symmetry of the proposed structure. Then large-signal experimental results verify the attenuation characteristics, as well as the thermal performance.**

***Index Terms*—Common-mode choke, differential-mode choke, electromagnetic interference (EMI), integration.**

I. Introduction

SWITCH-MODE power supplies and motor drives have been widely used for various cost, size, and performance advantages. However, because of high *di/dt* currents and high *dv/dt* voltages in the circuits, they generate high-differential-mode (DM) noise and common-mode (CM) noise. This often requires an electromagnetic interference (EMI) filter in order to meet relevant electromagnetic compatibility (EMC) standards. The EMI filter can be one of the largest components in the switch-mode converter system [1]. On the other hand, in recent years, switch-mode converters have been found in an increasing number of applications in telecom station, electric vehicles, aircraft and aerospace industry [2] and [3], where high power density is essential. Therefore, compact EMI filter design with good performance is desired to meet these new application requirements.

Manuscript received March 19, 2009; revised June 22, 2009. Current version published March 26, 2010. This work was primarily supported by the SAFRAN group and by the National Science Foundation Engineering Research Center shared facilities under Award EEC-9731677. Recommended for publication by Associate Editor J. Biela.

R. Lai is with the GE Global Research Center, Niskayuna, NY 12309 USA (e-mail: lai@ge.com).

Y. Maillet is with Converteam, Inc., Pittsburgh, PA 15238 USA (e-mail: yoann.maillet@converteam.com).

F. Wang is with the Min H. Kao Department of Electrical Engineering and Computer Science, The University of Tennessee, Knoxville, TN 37996-2100 USA (e-mail: f.wang@ieee.org).

S. Wang is with the Electrical Power Systems, GE Aviation Systems, Vandalia, OH 45377 USA (e-mail: shuowang@ieee.org).

R. Burgos is with ABB Inc., United Staes Corporate Research Center, Raleigh, NC 27606 USA (e-mail: rburgos@ieee.org).

D. Boroyevich is with the Center for Power Electronics Systems, Virginia Polytechnic Institute and State University, Blacksburg, VA 24061 USA (e-mail: dushan@vt.edu).

Color versions of one or more of the figures in this paper are available online at http://ieeexplore.ieee.org.

Digital Object Identifier 10.1109/TPEL.2009.2030803

Generally speaking, the EMI filter consists of two parts from the functionality standpoint: a DM filter and a CM filter. Among them, the DM chokes and CM chokes are sometimes the most bulky components. For example, in some applications for the aircraft, the DM capacitance is limited, therefore, a large DM inductance must be used to attenuate the DM noise. Because the leakage inductance of CM inductor is far from enough, separate DM inductors are needed.

There have been some previous research efforts made to reduce the size of the EMI chokes using an integration technique [4]–[7]. In [4], the integrated function is achieved by combination of an E-core and an I-core. The DM and CM inductances can be adjusted independently by changing the air gap between the two cores. However, the effective permeability is also reduced by the air gap, and, therefore, has an impact on the CM inductance. In [5], the leakage inductance of the CM choke is enhanced by stacking another toroid core adjacent to the windings that reduces the magnetic reluctance of the path for the leakage flux. However, in this case, the additional core is not fully utilized, and the DM inductance is not easy to control. Nan and Yugang [6] propose an integrated structure with one high-permeability core and two low-permeability cores. Although the inductor volume can be reduced by this approach, the number of components does not decrease when compared to the discrete structure, and the window area of the choke is not fully utilized. Boonma *et al.* [7] integrate the DM and CM suppression function with only one ferrite core and one powder core, but the winding structure is asymmetrical. According to the analysis of the CM choke [8], the asymmetrical structure may lead to unbalanced leakage inductance, which will impact the performance of the EMI filter in the high-frequency range due to the transformation between CM and DM [9].

This letter proposes a new approach for integrating the DM and CM chokes. Unlike previous papers, here both the inductor volume and the DM inductance are optimized, and the winding angle for each phase is symmetrical. The basic magnetic relationship for the proposed structure is analyzed and a prototype is built. The design concept is verified by small-signal measurement. A large-signal power test is carried out with a dc-fed motor drive (300 V/2 kW), and the experimental results verify the performance and the symmetry of the integrated structure. The thermal behavior of the integrated choke, which could be a concern for a low-volume structure, is also investigated in the experiment.

0885-8993/$26.00 © 2010 IEEE

Authorized licensed use limited to: University of Florida. Downloaded on December 30,2020 at 05:48:04 UTC from IEEE Xplore. Restrictions apply.

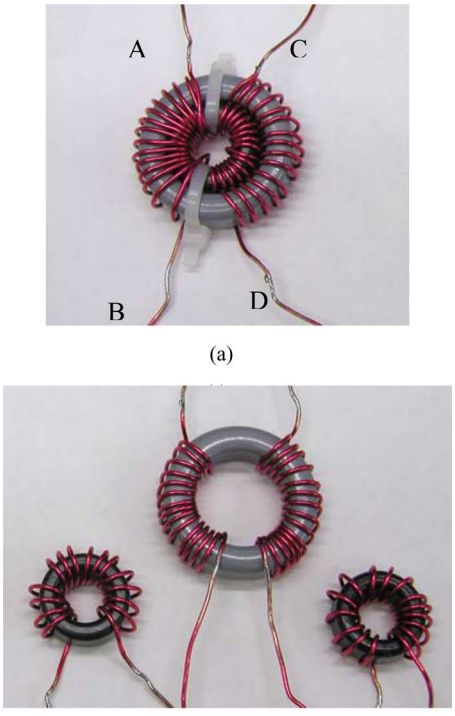

Fig. 1. (a) Integrated EMI choke. (b) Discrete EMI chokes.

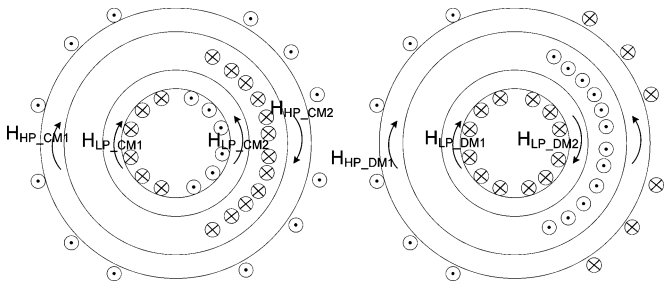

Fig. 2. Magnetic field intensity for CM current (left) and DM current (right) in integrated choke.

II. Proposed Structure and Analysis

Fig. 1(a) shows the core layout and the winding structure of the integrated EMI choke. It consists of a high-permeability core and a low-permeability core. For comparison, Fig. 1(b) shows the common discrete EMI chokes, which include one high-permeability core and two low-permeability cores. In the proposed structure, the low-permeability core is placed within the window of the high-permeability core. For the phase AB, the two cores share the same winding. For the other phase CD, the wire is wound in the shape of a figure eight when it crosses both cores. Fig. 2 shows a cross-sectional diagram and the flux direction of the integrated choke. As the figure indicates, when there is CM current going through the two phases, the magnetic fields generated by each phase will be canceled in the inner core but enhanced in the outer core. Assuming the windings of two phases have same number of turns and neglecting nonlinearity, the CM fluxes in the outer high-permeability core $\varphi_{\mathrm{HP\_CM}}$ and

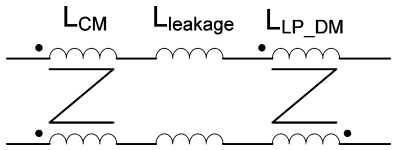

Fig. 3. Equivalent circuit for the integrated choke.

the inner low-permeability core $\varphi_{\mathrm{LP\_CM}}$ are given by

$$\begin{cases} \varphi_{\mathrm{HP\_CM}} = \varphi_{\mathrm{HP\_CM1}} + \varphi_{\mathrm{HP\_CM2}} = 2\varphi_{\mathrm{HP\_CM1}} \\ \varphi_{\mathrm{LP\_CM}} = \varphi_{\mathrm{LP\_CM1}} - \varphi_{\mathrm{LP\_CM2}} = 0 \end{cases} \tag{1}$$

where $\varphi_{\mathrm{HP\_CM1}}$ and $\varphi_{\mathrm{HP\_CM2}}$ are the CM fluxes in the outer core generated by each phase, and $\varphi_{\mathrm{LP\_CM1}}$ and $\varphi_{\mathrm{LP\_CM2}}$ are the CM fluxes in the inner core.

Therefore, the integrated choke will then behave like a single-core common-mode choke. The CM inductance is given by

$$L_{\mathrm{CM}} = \frac{N^2}{R_1} \tag{2}$$

where N is the number of turns for each phase winding, and R_1 is the magnetic reluctance [10] of the outer core. Here, the leakage inductance is ignored since it is much smaller than the self-inductance.

Similarly, when the DM current goes through the two phases, the fluxes in the outer core will be canceled except for the leakage, while the magnetic fields generated in the inner core are in the same direction. The DM fluxes in the outer core φ_{oDM} and the inner core φ_{iDM} are given by

$$\begin{cases} \varphi_{\mathrm{HP\_DM}} = \varphi_{\mathrm{HP\_DM1}} - \varphi_{\mathrm{HP\_DM2}} = 0 \\ \varphi_{\mathrm{LP\_DM}} = \varphi_{\mathrm{LP\_DM1}} + \varphi_{\mathrm{LP\_DM2}} = 2\varphi_{\mathrm{LP\_DM1}}. \end{cases} \tag{3}$$

The integrated choke in Fig. 1(a) can achieve higher DM inductance with fewer cores compared with the discrete version shown in Fig. 1(b). The total DM inductance can be given by

$$L_{\mathrm{DM}} = L_{\mathrm{leakage}} + L_{\mathrm{LP\_DM}} = L_{\mathrm{leakage}} + \frac{(2N)^2}{R_2} \tag{4}$$

where L_{leakage} is the leakage inductance of the outer choke, $L_{\mathrm{LP\_DM}}$ is the DM inductance of the inner choke, and R_2 is the magnetic reluctance of the inner core. The equivalent circuit of the integrated choke can be shown in Fig. 3.

In industry practice, the discrete DM inductors can be also implemented using only one low-permeability core with a coupled winding structure, but the proposed integrated structure still excels since it can reduce the footprint size of the inductors and the length of the copper wire. On the other hand, compared with the approach of using more number of turns on CM inductor to get higher leakage inductance for DM inductance, the proposed approach can achieve a smaller winding capacitance. But the winding structure of the integrated choke is complex and, therefore, leads to higher manufacturing cost.

III. Small-Signal Measurement

In order to verify the design concept, an integrated choke and the corresponding discrete chokes are built for test and

Authorized licensed use limited to: University of Florida. Downloaded on December 30,2020 at 05:48:04 UTC from IEEE Xplore. Restrictions apply.

TABLE I
CORE INFORMATION

	Manufacturer	Part Number	Outer Diameter	Inner Diameter	Height
Ferrite Core	Magnetics	42908TC	29 mm	19 mm	7.43 mm
Kool Mu Core	Magnetics	77121	16.5 mm	10.2 mm	6.35 mm

TABLE II
MEASUREMENT DATA AT 10 KHZ

	Integrated Choke	Discrete Chokes
Number of Turns	15	15
Wire Length	117 cm	140 cm
Volume	5.7 cm^3	9.5 cm^3
CM inductance	700 μH	732 μH
DM inductance	48.2 μH	28.7μH

comparison. A ferrite core and a Kool Mu core are used as the high-permeability core and low-permeability core, respectively. The detail core information is shown in Table I. The core size and inductance measurements at 10 kHz are shown in Table II. AWG #18 copper wire is utilized for the windings. Both inductor designs have the same number of turns. As Table II shows, the integrated choke can reduce the wire length and the total volume. For the discrete version, the leakage inductance of the CM choke is 13.3 μH, and the inductance of the two DM chokes is 15.4 μH. For the integrated choke, it is difficult to isolate the leakage inductance from the total DM inductance in the measurement. But based on the previous analysis, the DM inductance of the low-permeability choke is twice of the discrete version due to the mutual inductance of the two windings in the inner core, which is 30.8 μH. Therefore, the leakage inductance of the integrated choke can be achieved as 17.4 μH. Compared to the discrete version, the leakage inductance increases. It indicates that the coupling between the CM windings is lower in the integrated choke. The increment of leakage inductance is due to the embedded low-permeability core, which reduces the magnetic reluctance for the path of the leakage flux. The CM inductance also shows some difference, which is mainly caused by the permeability variation from core to core. Fig. 4 shows the impedance measurement results. The DM impedance of the integrated choke shows a higher value; up to 16 MHz. The integrated choke also shows a resonance point at around 11 MHz since it has higher equivalent parallel capacitance. Because there are twice numbers of turns on the integrated DM inductor than that of a single discrete DM inductor, the distance between winding turns on the integrated DM inductor is much smaller than that on the single discrete DM inductor. Based on the capacitance theory, the winding capacitance of the integrated DM inductor is, therefore, much larger than that of the single discrete DM inductor. Furthermore, the length of each turn of integrated DM inductor is longer than that of discrete inductor; therefore, it is expected that integrated DM winding capacitance is higher than that of the discrete one. Although the integrated DM inductor has a larger winding capacitance that the discrete one, the high frequency performance of the DM filter is strongly affected by mutual couplings [11], so larger winding capacitance may not lead to worse DM filter performance. For CM inductor, the number of turns is the same as that of the discrete one. The difference is the length of each turn, so the winding capacitance should not be too much different. Impedance measurements for both discrete and integrated inductors are shown in Fig. 4. They verified this analysis. The measured DM winding capacitance is 4.4 pF for integrated one and 1.8 pF for discrete one. CM winding capacitance is around 29 pF for discrete one and 33 pF for integrated one.

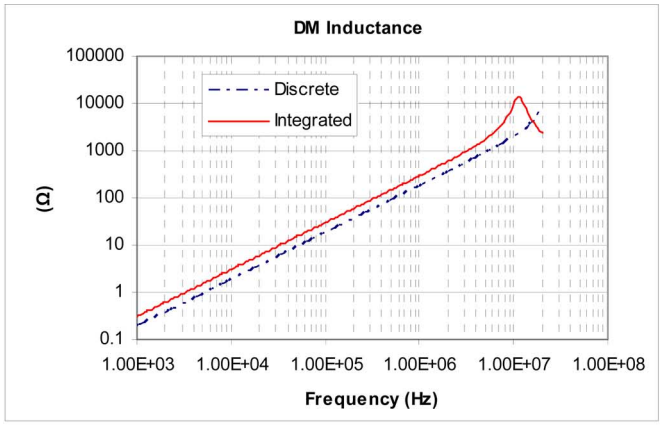

(a)

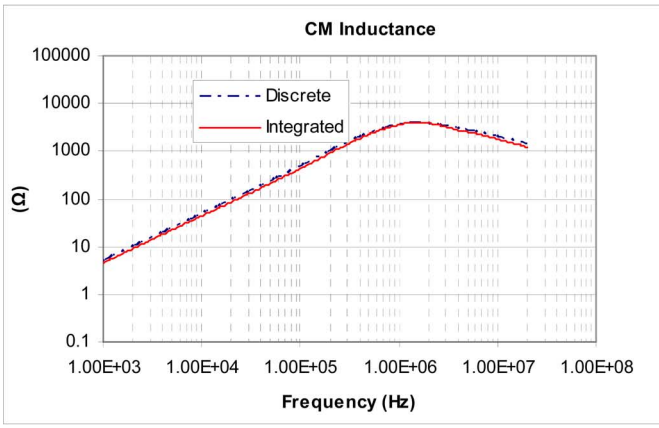

(b)

Fig. 4. Impedance measurement of the integrated choke and the discrete chokes. (a) DM inductance. (b) CM inductance.

In the high-frequency range, the grounding [12], coupling, and interaction with source impedance usually play dominant roles for the EMI noise; therefore, the resonance of the integrated choke may not lead to worse performance at the corresponding frequency. For the case in this letter, the concerned

Authorized licensed use limited to: University of Florida. Downloaded on December 30,2020 at 05:48:04 UTC from IEEE Xplore. Restrictions apply.

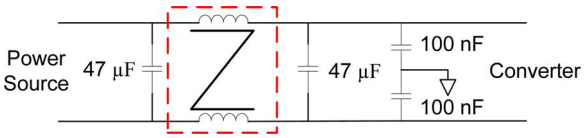

Fig. 5. Diagram of the Π type filter.

frequency range is from 10 kHz to 10 MHz, so, the effects of resonance between winding capacitance and the inductance can be ignored. Both CM inductors show similar performance for CM impedance. The small-signal measurement results agree with the analysis in the previous section.

One concern for the integrated choke is the possible impedance unbalance due to the structure, which can cause mode transformation between the CM and DM noises, leading to noise peaks at high frequencies [9]. In order to evaluate the balance of the proposed structure, the integrated choke is implemented into a "Π"-type filter, as shown in Fig. 5. The dashed frame in this figure represents the integrated choke. The DM capacitors are electrolytic type with the rating of 47 μF/450 V. And 100 nF/630 V ceramic capacitors are utilized for CM attenuation. A four-port network analyzer is used to measure the transmission coefficient [9] between the CM and DM of this filter. The measurement setup is shown in Fig. 6(a). The measurement is based on 50 Ω systems (source and load both are 50 Ω). It characterizes the transformation from DM–CM excitation on the left side to CM–DM response on the right side. The measurement results are shown in Fig. 6(b) and (c), which shows that the transformation between CM and DM is less than -75 dB for the whole measurement range. For comparison, the voltage insertion gain for both CM and DM are also included in Fig. 6(b) and (c). The results show that in most frequency range, the transformation is equal or lower than the corresponding CM and DM voltage insertion gain. This indicates that the filter structure is well balanced.

IV. Large-Signal Test

The experimental system for a large-signal test consists of a commercial dc-fed motor drive, a fan load that is connected to the drive via a 10 m shielded cable, a line impedance stabilization network (LISN), and a dc power supply. The measurement setup is shown in Fig. 7. The integrated choke is implemented into a "Π" network EMI filter. The CM capacitor C_Y is 100 nF and the DM capacitors (C_1/C_2) are 47 μF each. The dc bus voltage is 300 V and the fan load is running at 1.3 kW. The switching frequency is 12 kHz. Military Standard 461E is used, which defines the measurement frequency from 10 kHz to 10 MHz [13].

Figs. 8 and 9 show the DM noise and CM noise measurement results when using the noise separator [14]. Three cases are included in the figures: original noise without an EMI filter, noise with the EMI filter with discrete chokes, and the noise with the EMI filter with an integrated choke. The experimental results in Fig. 8 show that in the frequency range from 10 kHz to 500 kHz, the EMI filter with an integrated choke shows 5–10 dB improvement for the DM noise compared to the EMI filter with

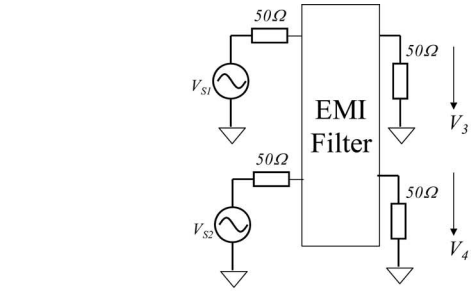

(a)

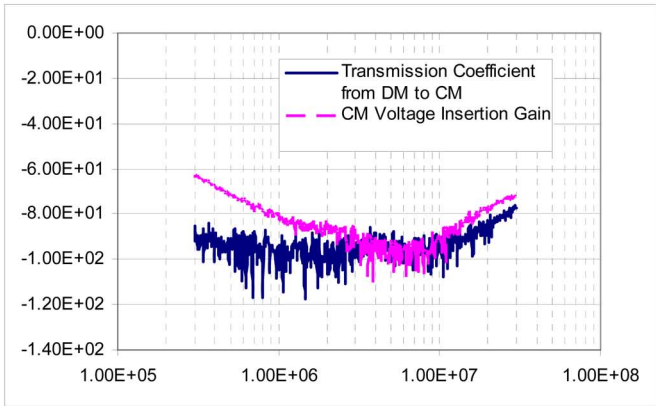

(b)

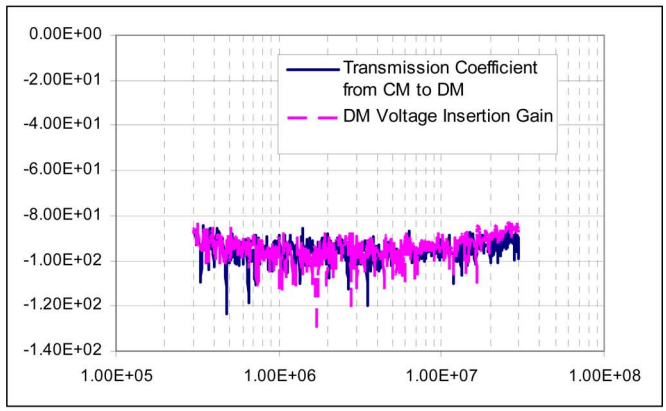

(c)

Fig. 6. Transmission coefficient measurement: (a) measurement setup, (b) transmission coefficient from DM to CM, and (c) transmission coefficient from CM to DM.

discrete chokes, which is due to the higher DM inductance. In a higher frequency range, the parasitic parameters and the coupling effect are dominant [11]. Furthermore, the resonant frequency of winding capacitance and DM inductance is higher than 10 MHz, the maximum concerned EMI frequency. Therefore, the two EMI filters have similar DM attenuation in the high-frequency range. The CM noise measurement results are shown in Fig. 9. The integrated choke and the discrete chokes show similar attenuation performance, which indicates that the integrated structure will not impact the CM performance. In addition, due to the parasitic in the measurement setup, the CM filter's high-frequency performance could be determined by other factors, for example, ground loop resonance [11], the

Authorized licensed use limited to: University of Florida. Downloaded on December 30,2020 at 05:48:04 UTC from IEEE Xplore. Restrictions apply.

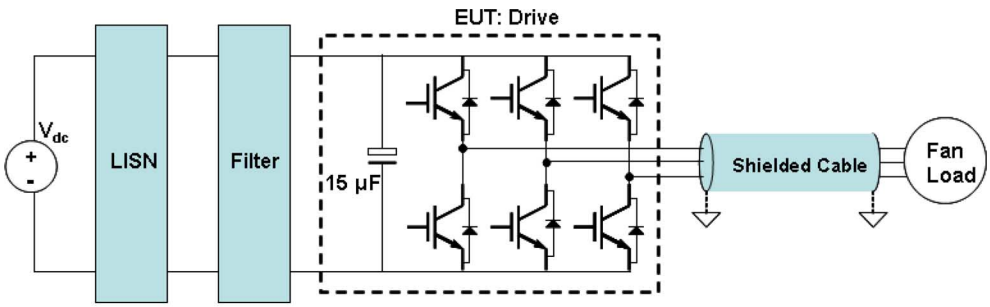

(a)

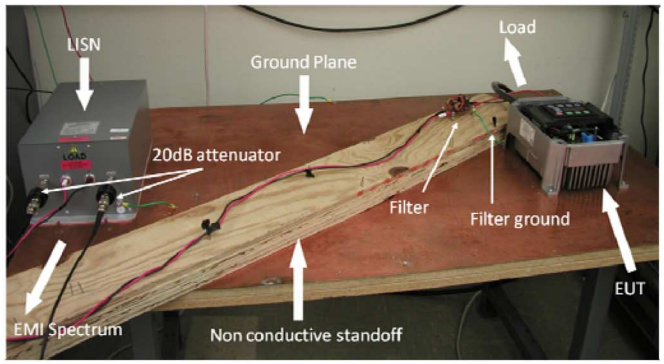

(b)

Fig. 7. (a) Circuit diagram of the experimental system. (b) Photograph of the system's setup.

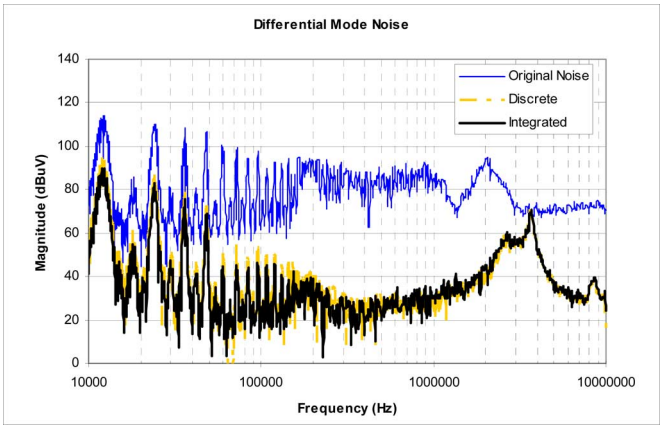

Fig. 8. DM noise measurement.

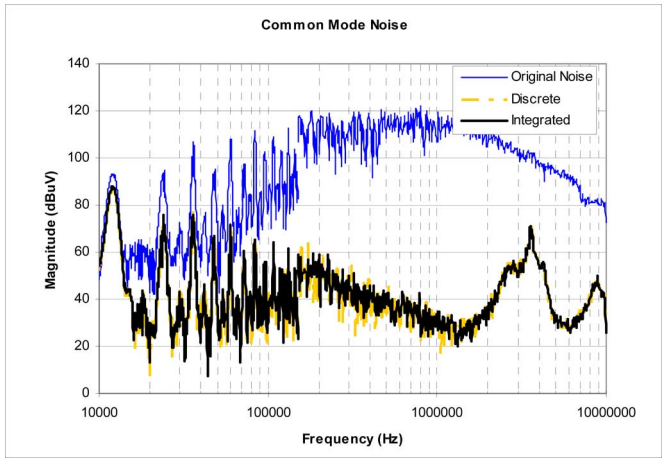

Fig. 9. CM noise measurement.

impedance of grounding wire [12], instead of the winding capacitance of inductors; therefore, the effects of CM winding capacitance do not always show up.

Thermal behavior is one of the key concerns for the high-density design. Compared to the discrete structure, the integrated choke has less copper due to the reduced wire length. At the same time, the heat dissipation area is reduced. The thermal performances for both structures are investigated in the experiments. Under rated condition, the filter achieved the steady-state temperature after 18 min operation. Fig. 10 shows the steady-state temperature measured by the thermal camera. The images are taken after 20 min of steady-state operation with natural cooling. As can be seen, the DM capacitor closest to the motor drive is the hottest component in both cases, because it absorbs most of the ripple current from the motor drive. Since the integrated choke has higher DM inductance, the DM capacitor with the integrated choke will absorb higher ripple current than the capacitor with the discrete chokes under the same operation conditions. Therefore, in the images, the DM capacitor with the integrated choke shows a higher temperature than the other. For the inductors, the temperature of the hot spot in the integrated choke is about 2 °C higher than the one in the discrete chokes. The temperature rise of the integrated choke is only 10% higher. This shows that the thermal dissipation is not an issue in this case.

Authorized licensed use limited to: University of Florida. Downloaded on December 30,2020 at 05:48:04 UTC from IEEE Xplore. Restrictions apply.

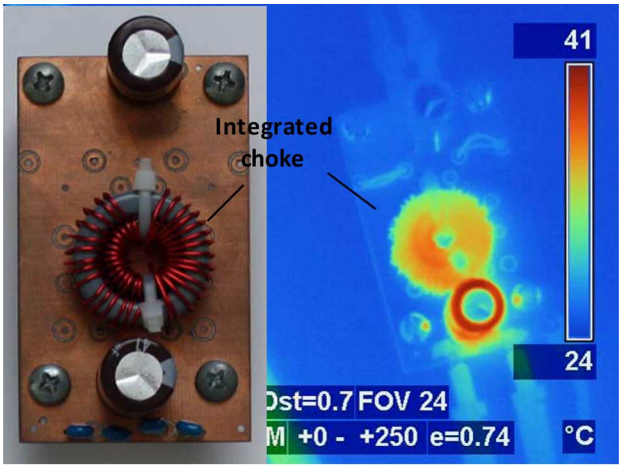

(a)

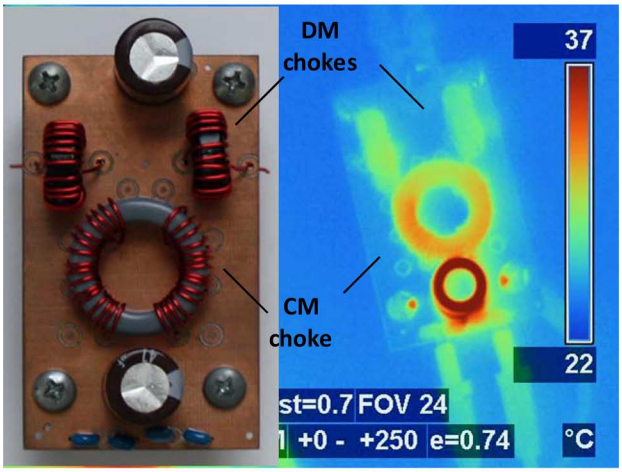

(b)

Fig. 10. Thermal measurement. (a) EMI filter with integrated choke. (b) EMI filter with discrete chokes.

V. Conclusion

This letter has presented a novel approach for the integration of CM and DM chokes. A low-permeability toroid core is embedded into the common-mode choke, and a special winding structure is utilized to achieve high DM inductance as well as good symmetry. The proposed structure features low volume, reduced copper wire length, and good impedance balance. But this structure will also lead to higher winding capacitance compare to the discrete chokes and probably requires higher labor cost. A laboratory-scale prototype is built with a ferrite CM core and a Kool Mu DM core. The design concept and the choke performance were verified by both small-signal measurement and a large-signal power test. When compared to the discrete version, the integrated choke shows a 40% volume reduction and a 16% copper wire reduction without degrading the EMI noise attenuation performance or causing serious thermal issues.

References

[1] R. M. Cuzner and J. C. VanderMeer, "Impacts to the power density of ship electric drives," *IEEE Power Electron. Soc. Newslett.*, vol. 16, no. 3, pp. 10–12, 2004.

[2] R. Lai, F. Wang, R. Burgos, Y. Pei, D. Boroyevich, B. Wang, T. A. Lipo, V. D. Immanuel, and K. J. Karimi, "A systematic topology evaluation methodology for high-density three-phase PWM ac-ac converters," *IEEE Trans. Power Electron.*, vol. 23, no. 6, pp. 2665–2680, Nov. 2008.

[3] D. Fu, P. Kong, S. Wang, F. C. Lee, and M. Xu, "Analysis and suppression of conducted EMI emissions for front-end LLC resonant DC/DC converters," in *Proc. IEEE Power Electron. Spec. Conf.*, Jun. 15–19, 2008, pp. 1144–1150.

[4] A. K. Upadhyay, "Integrated common mode and differential mode inductor device," U.S. Patent 5 313 176, May 17, 1994.

[5] T. P. Gilmore and G. Ray, "Method of configuring common mode/differential mode choke," U.S. Patent 6 768 408 B2, Jul. 27, 2004.

[6] L. Nan and Y. Yugang, "A common mode and differential mode integrated EMI filter," in *Proc. IPEMC 2006*, Shanghia, China, Aug., vol. 1, pp. 1–5.

[7] P. Boonma, V. Tarateeraseth, and W. Khan-ngern, "A new technique of integrated EMI inductor using optimizing inductor-volume approach," presented at the Int. Power Electron. Conf. (IPEC), Niigata, Japan, Apr. 2005.

[8] M. J. Nave, "On modeling the common mode inductor," in *Proc IEEE Int. Symp. Electromagn. Compat.*, Aug. 1991, pp. 452–457.

[9] S. Wang, J. D. van Wyk, F. C. Lee, and W. G. Odendaal, "Transformation between common mode and differential mode due to imperfect balance of EMI filters," in *Proc. CPES Annu. Power Electron. Conf.*, Blacksburg, VA, Apr. 2005, pp. 551–555.

[10] R. W. Erickson and D. Maksimovic, *Fundamentals of Power Electronics*, 2nd ed. New York: Springer-Verlag, Jan. 2001.

[11] S. Wang, F. C. Lee, D. Y. Chen, and W. G. Odendaal, "Effects of parasitic parameters on EMI filter performance," *IEEE Trans. Power Electron.*, vol. 19, no. 3, pp. 869–877, May 2004.

[12] S. Wang, Y. Maillet, F. Wang, D. Boroyevich, R. Lai, and R. Burgos, "Investigating the grounding of EMI filters in power electronics systems," in *Proc. IEEE Power Electron. Spec. Conf.*, 15–19 Jun. 2008, pp. 1625–1631.

[13] *Requirements for the Control of Electromagnetic Interference Characteristics of Subsystems and Equipment Department of Defense*, Military Standard 461E, Aug. 1999.

[14] S. Wang, F. C. Lee, and W. Odendaal, "Characterization, evaluation, and design of noise separator for conducted EMI noise diagnosis," *IEEE Trans. Power Electron.*, vol. 20, no. 4, pp. 974–982, Jul. 2005.

Authorized licensed use limited to: University of Florida. Downloaded on December 30,2020 at 05:48:04 UTC from IEEE Xplore. Restrictions apply.